



Cite this: DOI: 10.1039/d2fo00060a

## Astilbin from *Smilax glabra* Roxb. alleviates high-fat diet-induced metabolic dysfunction<sup>†</sup>

Tingwei Wang,<sup>a</sup> Yongli Ye,<sup>a</sup> Jian Ji,<sup>a</sup> Shuang Zhang,<sup>b</sup> Xingxing Yang,<sup>a</sup> Jiayuan Xu,<sup>a</sup> Jia-Sheng Wang,<sup>c</sup> Zhiyuan Chen,<sup>d</sup> Bangen Xia,<sup>e</sup> Hongfang Shen,<sup>e</sup> Ruowei Xia,<sup>e</sup> Wenqin Shi<sup>e</sup> and Xiulan Sun<sup>a</sup>  \*<sup>a</sup>

Overweight, obesity, and related diseases are currently the major public health problems worldwide. Astilbin, extracted from the rhizome of *Smilax glabra* Roxb., is known to have significant anti-inflammatory activity and hepatoprotective effect. Studies have shown that it can inhibit adipogenesis in adipocytes *in vitro*; however, the intervention benefits of astilbin against obesity and related diseases along with its associated mechanisms remain unknown. This study aimed to demonstrate the impact of astilbin consumption on the overall biochemical pattern of high-fat diet (HFD) mice by using a combined multi-omics approach. Our data indicated that astilbin reduced body weight, insulin resistance, and inflammation in mice fed an HFD. Astilbin improved HFD-induced gut microbial dysbiosis by decreasing the Firmicutes-to-Bacteroidetes ratio, by increasing beneficial bacteria such as *Alistipes* and *Muribaculum* and decreasing harmful bacteria including *Lachnospiraceae FCS020* group, *Coriobacteriaceae UCG-002*, and *Lachnospiraceae UCG-008*, resulting in enhanced intestinal carbohydrate and lipid metabolism. Meanwhile, astilbin protected the integrity of the intestinal barrier in HFD mice, increased short-chain fatty acid levels, and reduced metabolic endotoxemia. We further showed that astilbin attenuated hepatic lipid droplet aggregation and triglyceride accumulation in HFD mice, affected glutamate metabolism-related pathways, and enhanced hepatic ATP transduction pathways and attenuated xanthine metabolism pathways in mice, which were positively correlated with the abundance of *Alistipes* and negatively correlated with *Ruminococcaceae UCG-003*. The results highlighted that astilbin could be used as a prebiotic for the prevention of "gut–liver axis" damage and metabolic disruption in obese individuals.

Received 8th January 2022,  
Accepted 19th March 2022

DOI: [10.1039/d2fo00060a](https://doi.org/10.1039/d2fo00060a)  
[rsc.li/food-function](http://rsc.li/food-function)

### 1. Introduction

Over the past few decades, a growing number of epidemiological investigations have found an increase in the prevalence of overweight and obesity worldwide.<sup>1,2</sup> Over 40% of males and females (2.2 billion people) are currently overweight or obese;

based on the current trends, an estimated 40 million children will be obese or overweight in the next decade.<sup>3</sup> The China Population Nutrition and Chronic Disease Status Report 2020 concluded that the rate of overweight and obesity among residents of all age groups continued to rise, with more than 50% of adults in China being overweight or obese in 2016–2019, up from 42% in 2015.

The unreasonable dietary structure of the population, the continuous increase in the ratio of lipid energy supply, and a sedentary lifestyle are the direct causes of individual overweight and obesity.<sup>2,4</sup> They are important risk factors for chronic diseases, such as diabetes, nonalcoholic fatty liver, and a variety of cancers.<sup>5,6</sup> Multiple human studies found an association between food patterns characterized by high-fat diet (HFD) choices and the prevalence of obesity.<sup>3,7,8</sup> HFD rapidly and reproducibly alters the composition and function of the intestinal microbiota, and the resulting ecological dysregulation alters the function of the intestinal barrier and activates inflammatory pathways that may promote insulin resistance and metabolic syndromes such as obesity by altering insulin receptor signaling.<sup>9–11</sup>

<sup>a</sup>School of Food Science, State Key Laboratory of Food Science and Technology, National Engineering Research Center for Functional Foods, School of Food Science Synergetic Innovation Center of Food Safety and Nutrition, Joint International Research Laboratory on Food Safety, Jiangnan University, Wuxi, Jiangsu 214122, China. E-mail: sxlzz@jiangnan.edu.cn

<sup>b</sup>State Key Laboratory of Food Science and Technology, Jiangnan Analysis and Testing Center, Jiangnan University, Wuxi, Jiangsu 999078, China

<sup>c</sup>Department of Environmental Health Science, College of Public Health, University of Georgia, Athens, GA, USA

<sup>d</sup>College of Chinese Medicine, Macau University of Science and Technology, Macau, 999078, China

<sup>e</sup>Ningbo Xiabang New Pharmaceutical Technology Co., Ltd, Ningbo, Zhejiang, 315000, China

<sup>†</sup>Electronic supplementary information (ESI) available. See DOI: <https://doi.org/10.1039/d2fo00060a>

*Smilax glabra* Roxb., a traditional Chinese herb also available as a food, has been reported to have several beneficial effects, including antiviral, antioxidant, anticancer, and anti-inflammatory.<sup>12,13</sup> Astilbin is the main active substance in the rhizome of *S. glabra* Roxb., which has various functions such as anti-inflammatory activity and antioxidant effect.<sup>14</sup> Astilbin has been reported to reduce body weight and protect against liver injury in obese mice,<sup>15</sup> but most of these studies were observational and the effect of astilbin consumption on gut microbes has not been reported yet.

In this study, we investigated whether astilbin consumption could reduce obesity in HFD-fed mice. Using a combination of lipidomics, gut microbiomics, and metabolomics, we explored the ability of astilbin to characterize the HFD-fed individual organs and the overall gut–liver axis, as well as to improve host metabolism. We found that astilbin modulated gut microbes in HFD mice, ameliorated gut–liver axis metabolic disturbances, and reduced body weight and liver lipid accumulation in mice. Thus, our data suggested that astilbin had great potential as a potential prebiotic for treating obesity and its complications.

## 2. Methods and materials

### 2.1. Chemicals

Astilbin (from *S. glabra* Roxb., HPLC ≥98%) was obtained from Shanghai Yuanye Biotechnology Co., Ltd, China (see the ESI† for its characterisation). It was dissolved in DMSO and diluted with physiological saline. The diets in the Chow and Chow + Astilbin groups consisted of 10% lipids and 15% proteins, while the diet in the HFD group consisted of 60% lipids, 25.5% carbohydrates, and 15.1% proteins (Jiangsu Xietong Pharmaceutical Bio-engineering Co., China). Blood glucose test strips were purchased from Roche, UK. The mouse tumor necrosis factor α (TNF-α), interleukin-6 (IL-6), and interleukin-10 (IL-10) enzyme-linked immunoassay kits were purchased from Elabscience, China. All metabolomics- and lipidomics-related reagents and standards were obtained from Sigma-Aldrich. The antibodies used for western blot analysis were ZO-1 (Proteintech, 21773-1-AP, China) and β-actin (Beyotime, AF0003, China).

### 2.2. Animal study

All animal procedures were performed in accordance with the Guidelines for Care and Use of Laboratory Animals of Jiangnan University and the experiments were approved by the experimental animal ethics committee of Jiangnan University, and the animal ethics number for this experiment is JN. No20191030c1280130 [301]. Thirty-two 5-week-old C57BL/6J male mice were randomly divided into four groups after receiving them for 2 weeks: Chow group (Chow), astilbin consumption group (Chow + Astilbin), an HFD group, and an HFD with astilbin consumption group (HFD + Astilbin). In the two astilbin consumption groups, the mice were gavaged with 20 mg astilbin per kg body weight (b.w.) per day. All mice had free

access to their feed and water, and their body mass and food consumption were recorded once a week for 9 weeks. All samples and tissues were carefully collected and then stored at –80 °C until analysis.

### 2.3. Intraperitoneal glucose tolerance test (IPGTT)

IPGTT was performed at the end of modeling in C57 mice. The mice were fasted without water for 16 h the night before, weighed early next morning, and injected intraperitoneally with 2.0 g of glucose water per kg of body weight. Blood was collected from the tail vein 0 min before and 30, 60, 90, and 120 min after glucose loading, and the blood glucose levels were measured using a Roche glucometer. The area under the glucose curve (AUC) was calculated as an index to evaluate glucose tolerance.

### 2.4. Detection of serum biochemical indicators

The serum biochemical indices of triglyceride (TG), low-density lipoprotein (LDL), high-density lipoprotein (HDL), alanine aminotransferase (ALT), and aspartate transaminase (AST) were measured using a Murray Biochemistry Analyzer 800.

### 2.5. Hematoxylin and eosin staining

Liver and ileal samples were fixed in 10% neutral-buffered formalin solution for 24 h, and then washed with phosphate-buffered saline and stored in 70% ethanol. After embedding using paraffin, the tissues were cut to 4 μm thickness and immediately stained using a hematoxylin and eosin (H&E) staining kit (Beyotime, China).

### 2.6. Oil Red O-stained liver

The liver tissues were collected and placed on dry ice for freezing. Then, the samples were cut to 7 μm thickness, fixed in 10% formalin for 10 min, and washed with distilled water, followed by a 30 s immersion wash in 60% isopropanol. The sections were placed in Oil Red O (Sigma-Aldrich, USA) solution (0.5% in 60% isopropanol) for 15 min. The nuclei were slightly washed with 60% isopropanol and distilled water and then restained with a Mayer hematoxylin staining solution for 2 min.

### 2.7. Enzyme-linked immunosorbent assay

To determine the levels of TNF-α, IL-6 and IL-10 in serum, we centrifuged the serum and quantified inflammatory factors using enzyme-linked immunosorbent assay (ELISA) kits (Elabscience, China). ELISA results were quantified using a microplate reader set to test at a wavelength of 450 nm and corrected for absorbance at 540 nm according to the manufacturer's instructions. All experiments were repeated at least three times.

### 2.8. Measurements of short-chain fatty acids (SCFAs)

The SCFA content in feces was determined by gas chromatography-time-of-flight mass spectrometry (GC-TOF/MS) (a Pegasus BT gas chromatography TOF mass spectrometer,

LECO, USA) according to the method proposed by Liu *et al.*<sup>16</sup> Briefly, 40 mg of the sample was extracted with 50  $\mu$ L of saturated KHSO<sub>4</sub> solution. Then, 50  $\mu$ L of internal standard (acetic acid-d4, 0.1 mg mL<sup>-1</sup> in deionized water) was added and shaken for 30 s. Further, 500  $\mu$ L of acetonitrile solution was added, and the mixture was vortexed, pulverized, and centrifuged.

The parameters of the GC-TOF/MS method for detecting SCFAs were as follows: ionization mode, EI; emission current, 1 mA; electron energy, 70 eV; inlet temperature, 250 °C; injection volume, 1  $\mu$ L; source temperature, 210 °C; detector voltage, 2000 V; initial temperature, 60 °C; initial time, 1 min; rate, 15 °C min<sup>-1</sup>; final temperature, 240 °C; hold time, 10 min; sample method, temperature, 250 °C; spectral ratio = 10 : 1; carrier mode, constant current; value, 1 mL min<sup>-1</sup>; column, DB-5 MS column, 30 m × 0.25 mm id; and 0.25  $\mu$ m film thickness (Agilent, USA).

## 2.9. Lipidomic analysis

The liver lipids were extracted according to the standard operating procedures of the Fiehn Laboratory. Briefly, 40 mg of liver tissue was extracted with 1.1 mL of extraction solution [methyl *tert*-butyl ether/methanol/H<sub>2</sub>O (65 : 22 : 16, v/v/v)] and the mixture was vortexed, pulverized, and centrifuged. For further analysis, the dried nonpolar phase extracts were reconstituted in acetonitrile (ACN)/isopropanol (IPA)/H<sub>2</sub>O (65 : 30 : 5, v/v/v). The internal standard mixture, containing lysophosphatidylcholine (LPC) (19 : 0 at 0.28  $\mu$ g mL<sup>-1</sup>), sphingomyelin (SM) (12 : 0 at 0.28  $\mu$ g mL<sup>-1</sup>), chenodeoxycholic acid-d4 at 0.56  $\mu$ g mL<sup>-1</sup>, TAG (45 : 0) at 0.94  $\mu$ g mL<sup>-1</sup>, free fatty acids (FAs), C16:0-d3 at 0.94  $\mu$ g mL<sup>-1</sup>, and C18:0-d3 at 0.94  $\mu$ g mL<sup>-1</sup>, was added to each sample before lipid extraction.<sup>17</sup>

Further, we performed a lipidomic analysis of mouse liver lipids by the method proposed by Xu *et al.*<sup>18</sup> A Q-Trap 5500 mass spectrometer system (AB Sciex, USA) was used for pseudotargeted lipidomic analysis (Xuan *et al.*, 2018). A liquid-phase method was used as follows: column: BEH C8 column, 2.1 × 100 mm<sup>2</sup> id, 1.7  $\mu$ m film thickness (Waters, USA); mobile phases A and B: ACN/H<sub>2</sub>O (60 : 40, v/v) and IPA/ACN (90 : 10, v/v), both containing 10 mM ammonium acetate; flow rate: 0.26 mL min<sup>-1</sup>; and column temperature: 55 °C. The elution gradient was set as follows: 0 min, 32% B; 15.5 min, 85% B; 15.6 min, 97% B; and kept at 97% B until 18 min before ramping down to 32% B at 18.1 min. The flow rate was 0.26 mL min<sup>-1</sup>, and the injection volume was 2  $\mu$ L. For the mass spectrometer system, the pressure range of curtain gas, gas 1 and gas 2 was 0.41 MPa. The electrospray ion source temperature and spray voltage were set to 550 °C and 5500 V for the ESI+ and ESI- modes, respectively.<sup>19</sup> The lipids monitored by the pseudo-targeted lipidomics method were processed quantitatively (version 1.6, AB Sciex, Canada) using Analyst software.

## 2.10. Metabolomic analysis

The metabolites were extracted and assayed following the standard operating procedures of the Fiehn Laboratory.<sup>20</sup> In this

study, 40 mg liver tissue was extracted with 1 mL of extraction solution [acetonitrile/isopropanol/H<sub>2</sub>O (3 : 3 : 2, v/v)], and the mixture was vortexed, pulverized, and centrifuged. Subsequently, 450  $\mu$ L of the metabolic extract was saved and then dried in a Savant high-capacity Speedvac plus concentrator (Thermo Fisher Scientific, USA) for 6 hours. Then, 80  $\mu$ L of 20 mg mL<sup>-1</sup> methoxylamine hydrochloride was added to the dried metabolites and incubated in a constant-temperature metal bath at 80 °C for 20 min. After cooling to room temperature, 100  $\mu$ L of MSTFA (containing 1% trimethylchlorosilane, v/v) was added to the reaction system and incubated at 70 °C for 1 h.

The parameters of the GC-TOF/MS method for detecting metabolites were as follows: mass spectrometry conditions—ionization mode, EI; emission current, 1 mA; electron energy, -70 eV; interface temperature, 280 °C; and source temperature, 230 °C; chromatographic conditions—initial temperature, 80 °C; initial time, 4 min; rate, 6 °C min<sup>-1</sup>; final temperature, 300 °C; and hold time, 10 min; and injector method—temperature, 250 °C; injection volume, 1  $\mu$ L; spectral ratio, 10 : 1; carrier mode, constant current; value, 1 mL min<sup>-1</sup>; DB-5 MS column, 30 m × 0.25 mm id; and 0.25  $\mu$ m film thickness (Agilent). The MS data were obtained in the full-scan mode with *m/z* in the range of 50–600 at a rate of 20 spectra per s.

After raw data were converted into abf format using an ABF converter (<https://www.reifycs.com/AbfConverter/index.html>), MS DIAL software equipped with the Fiehn Library was used for peak extraction, filtering, calibration of the data baseline, peak alignment, deconvolution analysis, peak identification, and integration of peak heights.<sup>20</sup> Subsequently, each metabolite peak in all samples was normalized using the SERRF normalization method based on the quality control samples.

## 2.11. 16S rRNA gene sequencing

DNA in feces was extracted and purified using a ZymoBIOMICS DNA Microprep Kit (Zymo Research, USA). Amplification of bacterial 16S rRNA sequencing genes (V3–V4 region) was carried out using primers (515F, 5'-GTGYCAGCMGCCGCGTAA-3'; 806R, 5'-GGACTACHVGGGTWTCTAAT-3'). The amplification products were quantified, pooled, and sequenced using the Hiseq Rapid SBS Kit v2 (500 cycles, Illumina, USA) with PE250 sequencing. FLASH (v1.2.8) was used to stitch the double-ended sequences and QIIME (v2.0) was used for quality filtering. The sequences with 97% similarity were classified as an operational taxonomic unit according to the UPARSE algorithm and were analyzed. The microbial sequencing clustered OTU tables were filtered using QIIME software, leaving the results in the greengene database. After the OTU was flattened and normalized, the sample microbial composition was analyzed for diversity using R, Prism software. Gene function analysis was performed on the OTU tables using PICRUSt software (<https://huttenhower.sph.harvard.edu/galaxy/>).

## 2.12. Statistical analysis

All experimental data were presented as means ± standard deviation. The significance was analyzed using SPSS 20 with a

two-tailed Student's *t*-test or one-way analysis of variance with uncorrected Fisher's least significant difference test. A probability value of  $P < 0.05$  indicated a statistically significant difference.

### 3. Results

#### 3.1. Astilbin reduced HFD-induced weight gain and insulin resistance

We conducted the study in 32 8-week-old male C57BL/6J mice fed with normal chow (Chow group) and fed with HFD (HFD group) for 9 weeks. Half of the mice in both groups received daily gavage of astilbin until the end of the experiment. After 9 weeks of astilbin treatment, the mice in the HFD + Astilbin group exhibited significant weight loss in comparison with mice in the HFD group, while the mice in the Chow + Astilbin group had insignificant body weight changes compared with the mice in the Chow group (Fig. 1a). After the 9-week experiment, the total energy intake of all mice was calculated. The energy consumption of mice in the Chow + Astilbin group was higher than that in the Chow group, while the energy consumption in the HFD + Astilbin group was slightly lower than

that in the HFD group, indicating that astilbin treatment-induced weight loss in HFD mice might be related to a reduction in calorie consumption (Fig. 1b). After sacrificing the mice, the organ coefficients were measured. The mice in both the Chow and HFD groups did not show significant changes in liver organ coefficients after astilbin consumption (Fig. 1c). The assessment of glucose clearance by IPGTT (Fig. 1d and e) showed that astilbin consumption improved glucose tolerance levels in HFD mice ( $P = 0.114$ , Fig. 1e). Thus, our results suggested that astilbin treatment had a positive effect in terms of improving HFD-induced weight gain and insulin resistance.

#### 3.2. Astilbin reduced HFD-induced blood lipids, liver damage, and liver lipid accumulation in mice

Patients with metabolic syndrome usually have increased serum liver enzymes and disorders of hepatic lipid metabolism.<sup>9</sup> Astilbin consumption decreased the blood lipids in HFD mice, revealed by a lower level of TG in serum (Fig. 2c). In parallel, the HDL level in serum significantly increased in both mice in the chow and HFD groups after astilbin treatment. No significant changes in LDL levels were observed in the HFD +

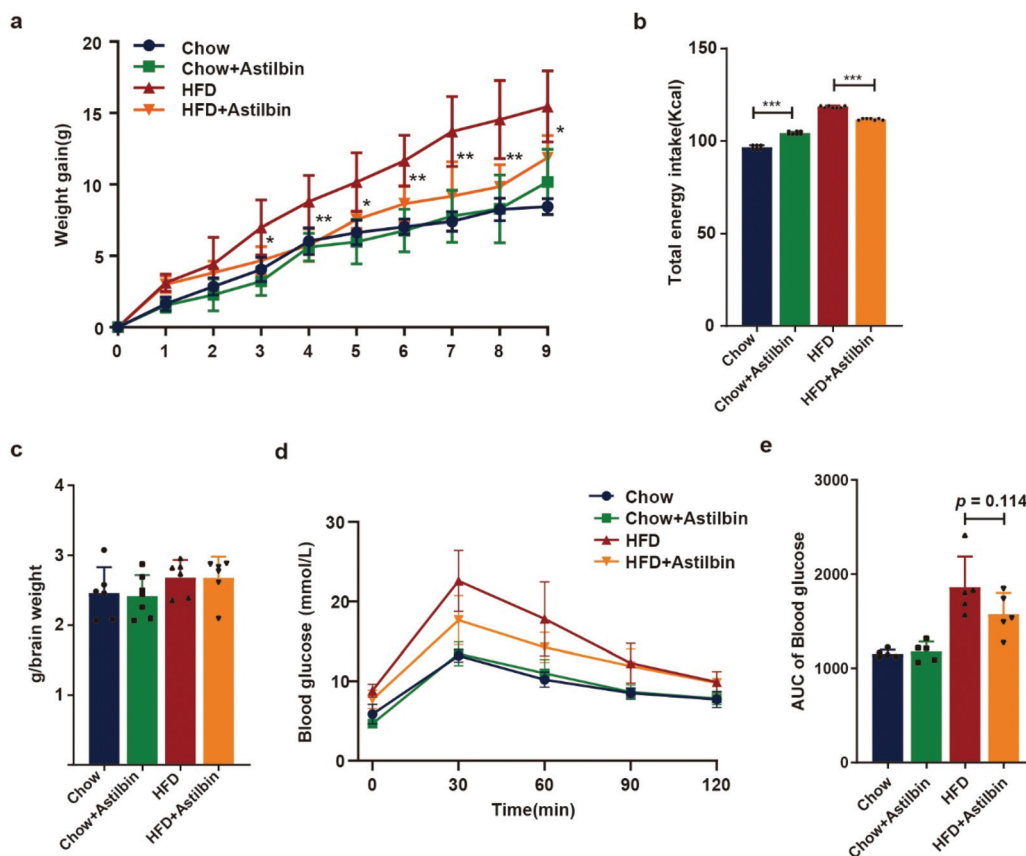


**Fig. 1** Effect of astilbin consumption on body weight and glucose tolerance in HFD-fed mice. (a) Body weight gain ( $n = 7\text{--}8$  per group). (b) Total energy intake of mice after 9 weeks ( $n = 7\text{--}8$  per group). (c) Liver organ coefficients of each group of mice (liver mass/brain mass). (d) IPGTT detected the changes in glucose homeostasis in mice ( $n = 5$  per group). (e) AUC of IPGTT.

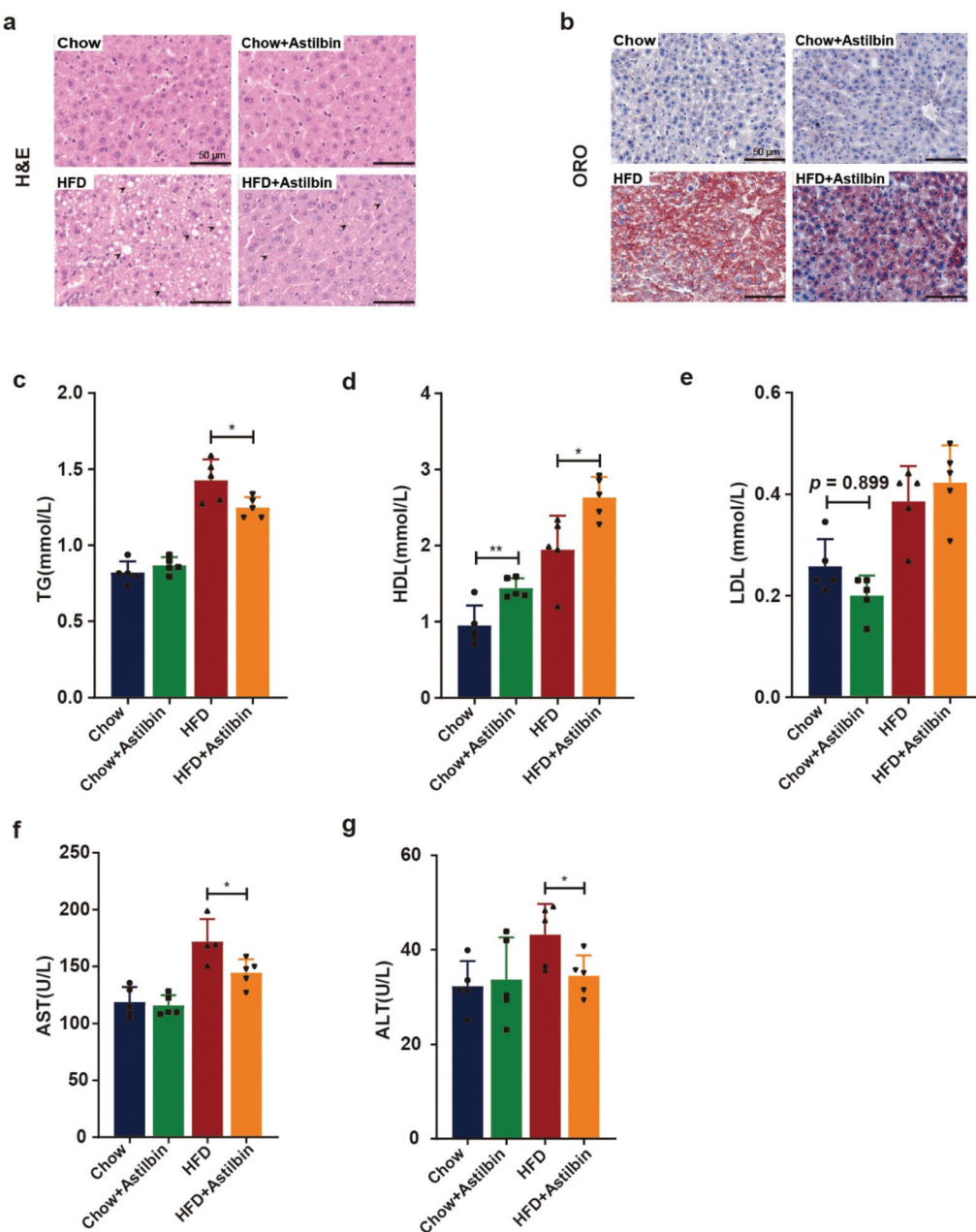


**Fig. 2** Effects of astilbin consumption on blood lipids, liver damage, and liver lipid accumulation in HFD-induced mice. (a) H&E staining of the livers in the four groups of mice. (b) Oil Red O staining of the livers in the four groups of mice. (c–g) Astilbin reduced the levels of serum TG, AST, and ALT and increased the level of HDL in mice.

Astilbin and HFD groups, while a trend of decreasing LDL levels was observed in mice in the Chow group after astilbin intake (Fig. 2d and e). The serum concentrations of AST and ALT significantly reduced in mice in the HFD + Astilbin group compared with those in the HFD group, but no significant difference was found between the Chow and Chow + Astilbin groups (Fig. 2f and g). In contrast, the Oil Red O staining and H&E staining of liver tissues showed that astilbin consumption caused a significant reduction in the liver lipid content in HFD mice (Fig. 2a and b).

### 3.3. Astilbin reduced HFD-induced TG accumulation in the liver

Since a reduction in hepatic lipid droplet aggregation in HFD mice due to astilbin consumption was observed, we further examined the lipid composition of mouse liver using lipidomics. A total of 837 different lipids were detected, including 318 triglycerides, 134 phosphatidylethanolamines (PEs), 79 phosphatidylcholines (PC), and other lipid classes (Fig. 3a). The relative quantification results indicated that

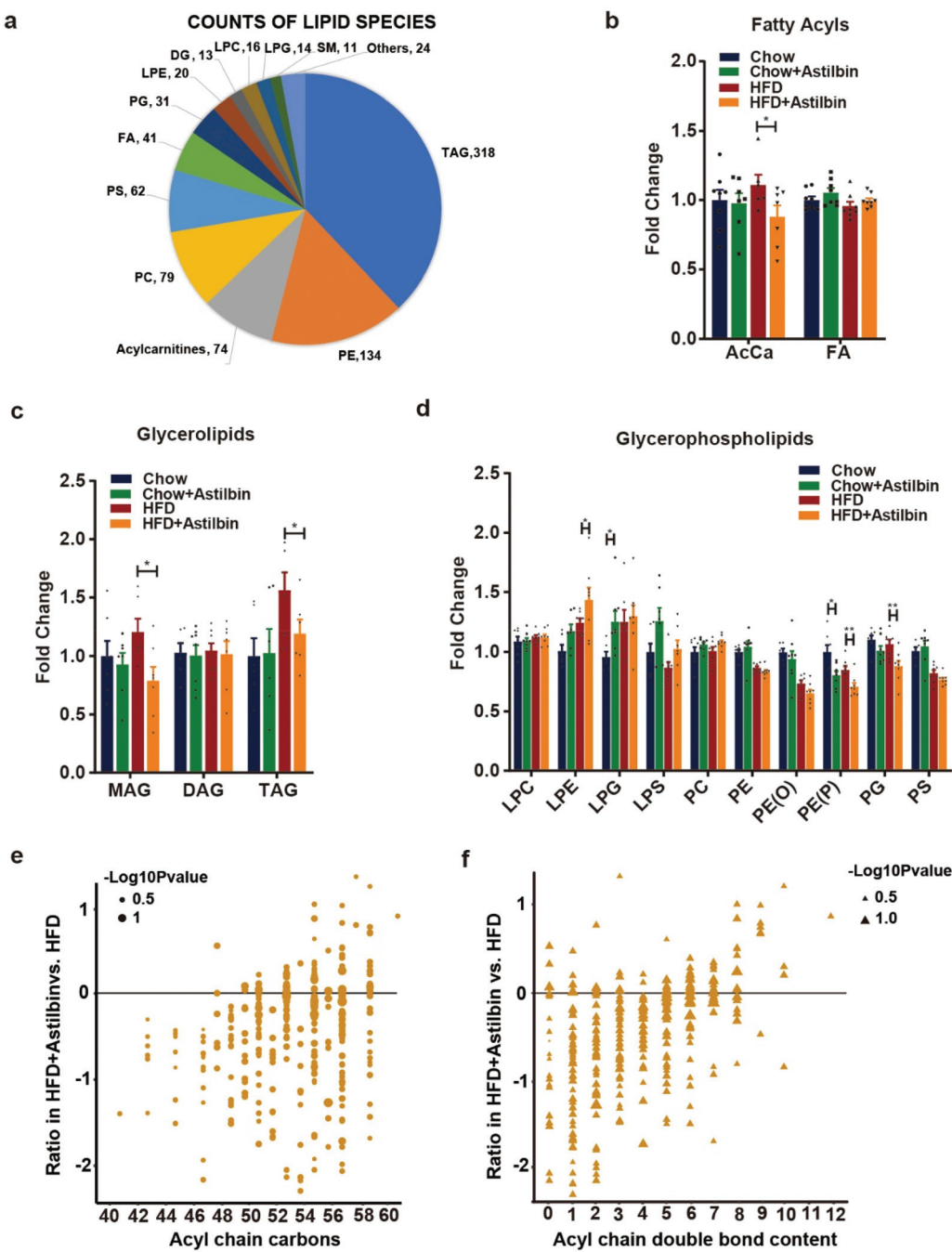


**Fig. 3** Changes in the overall lipid composition and distribution after astilbin consumption. (a) Distribution of all lipid classes detected. (b-d) Intensity fold change of fatty acyls (b), glycerolipids (c), and glycerophospholipids (d). (e and f) TAG pattern in the HFD + Astilbin group versus the HFD group. Each dot or triangle represents a distinct TAG, organized along the x-axis based on the acyl-chain carbon number (e) or double-bond content (f). Size of each dot or triangle is proportional to the significance values, which are displayed as  $-\log_{10}(P\text{ value})$ . Fold change = values/means of the Chow group.

astilbin consumption led to a significant decrease in the levels of monoglycerides (MAG), triacylglycerols (TAG), hexosylceramide (HCER), alkenyl-phosphatidylethanolamines (PE-P), and phosphatidylglycerols (PG) and an increase in the level of lysophosphatidylethanolamine (LPE) in HFD mice. Meanwhile, only ceramide (CER) and lysophosphatidyl-glycerols (LPG) were upregulated and PE-P levels were down-

regulated in the Chow + Astilbin group compared with the Chow group (Fig. 3b-d and Fig. S2b†). We used a  $P$  value  $<0.05$  as the cutoff to further reveal the effect of astilbin consumption on the changes in the hepatic lipid levels in HFD mice. A total of 173 species changes were observed, indicating that astilbin had a strong effect on liver lipid metabolism in HFD mice (Fig. 3a).

We sorted TAG lipids according to *P* values to investigate the effect of astilbin consumption on the composition of fatty acyl chains in HFD mice. The levels of a large number of TAGs decreased in the HFD + Astilbin group, with a significant reduction in seven species (Fig. S2d†). Astilbin consumption induced a significant reduction in the levels of saturated fatty acids (SFAs) in the liver of HFD mice, while the levels of mono-unsaturated fatty acids (MUFAs) and polyunsaturated fatty acids (PUFAs) did not change significantly (Fig. S2c†). TAG species with lower carbon numbers and double-bond content have been correlated with an enhanced risk of type II diabetes (T2D).<sup>21</sup> The results showed astilbin-induced decreased levels of TAG species with relatively low double-bond content and acyl-chain carbon number in the livers of HFD mice, suggesting that astilbin consumption reduced the number of TAG species that might be detrimental to the treatment of T2D (Fig. 3e and f). Glycerophospholipids are the most abundant class of phospholipids in organisms and have physiological functions such as signaling and synthesis of cell membranes. Moreover, astilbin consumption altered the levels of various glycerophospholipids in the livers of HFD mice. We ranked the *P* values and screened and examined the top 20 species individually. We found that the levels of 11 lipids were significantly reduced (four PE-P lipids, three PE-O lipids, two LPG lipids, one PE lipid, and one PS lipid) and the levels of nine lipids significantly increased (six PC lipids, one PE-O lipid, one LPC lipid, and one PS lipid) after astilbin intervention (Fig. S2e†).

#### 3.4. Astilbin reduced HFD-induced intestine damage and disruption of short-chain fatty acid metabolism

Excessive consumption of HFD can cause varying degrees of intestinal inflammation and increase intestinal permeability. The histopathological sections of the ileum showed that astilbin consumption increased the ileal villus height and crypt depth in HFD mice (Fig. 4a and b). Meanwhile, the protein expression of zonula occluden-1 (ZO-1) in the ileum was further examined. Similar to most reports, HFD significantly decreased the protein level of intestinal ZO-1 in mice, while astilbin consumption improved the level of ZO-1 in HFD mice. No significant change in the levels of ZO-1 protein was observed in mice in the Chow group after astilbin consumption. Further, we tested the levels of inflammatory factors in mouse serum. We found that astilbin significantly decreased the levels of pro-inflammatory factors TNF- $\alpha$  and IL-6 and increased the levels of the anti-inflammatory factor IL-10 in HFD-fed mice. In conclusion, astilbin enhanced intestinal integrity, increased SCFA levels, and attenuated systemic inflammatory responses in HFD-fed mice (Fig. 4g–i).

Accumulating evidence shows that SCFAs play a key role in maintaining intestinal and metabolic health, and the increased production of microbial SCFAs can be considered beneficial for health.<sup>22</sup> The overall levels of SCFAs in both groups of astilbin consumption exhibited a significant increasing tendency compared with those in the Chow and HFD

groups (Fig. 4e and f). Astilbin consumption significantly increased the levels of butyric acid and isobutyric acid in the feces of mice following both dietary patterns, as well as the levels of valeric acid, reflecting the specific protective effect of astilbin on the intestine.

#### 3.5. Astilbin reversed HFD-induced gut microbial dysbiosis

The 16s rRNA-based high-throughput sequencing was used to assess astilbin consumption for changes in the cecal microbiota of mice fed both diets. Similar to the results previously reported in the literature, HFD caused alterations in the intestinal microbiota, resulting in a decrease in alpha-diversity: the Chao1, Simpson, and Shannon indexes.<sup>23,24</sup> Interestingly, astilbin increased the total number and diversity of microbial species in the gut of HFD mice, while no significant change was observed in the Chow + Astilbin group compared with the Chow group (Fig. 5a–c). Meanwhile, the principal component analysis (PCA) results for  $\beta$ -diversity showed differences in the microbial status of the four groups, suggesting that astilbin consumption affected the composition of the microbial community in mice (Fig. 5d).

Next, the relative abundance of microorganisms at the phylum and genus levels was analyzed. Astilbin consumption decreased the Firmicutes-to-Bacteroidetes ratio and Proteobacteria levels, which are thought to be positively associated with the occurrence of metabolic syndrome. Meanwhile, astilbin increased the levels of Epsilonbacteraeota and Deferribacteres in the intestine of mice fed both diets (Fig. 5e). Further, the specific genus affected by astilbin was identified. The abundance of *Hydrobacter*, *Ruminiclostridium\_9*, *Muribaculum*, and *Alistipes* increased, while that of *Ruminococcaceae\_UCG-003*, *Lachnospiraceae\_NK4A136* group, *Lachnospiraceae\_FCS020* group, and *Coriobacteriaceae\_UCG-002* decreased (Fig. 3a and b).

Tax4Fun analysis based on the KEGG database was used to predict the metabolic function so as to understand how astilbin-mediated changes in the gut microbiota of HFD mice regulated metabolism. By prediction, significant changes in the three levels of intestinal pathways were found in HFD mice. The LDA score of the level 2 metabolic pathway showed that astilbin intake significantly enhanced the levels of amino acid metabolism, carbohydrate metabolism, and lipid metabolism in HFD mice (Fig. 5f). In addition, Fig. 3c shows seven important metabolic pathways at level 3, indicating that astilbin enhanced the metabolism of SCFAs, carbohydrate metabolism, and amino acid metabolism (Fig. S3c†).

#### 3.6. Astilbin reversed HFD-induced liver metabolic dysfunction

As the reversal of HFD-induced intestinal damage by astilbin and gut microbiota disruption was observed, we further investigated the effect of astilbin on liver metabolism in mice using metabolomic analysis. A total of 183 metabolites were successfully identified and quantified by the GC-TOF/MS assay. PCA was performed. The score plots of the four groups in PCA are shown in Fig. 6a. The observed difference between the HFD

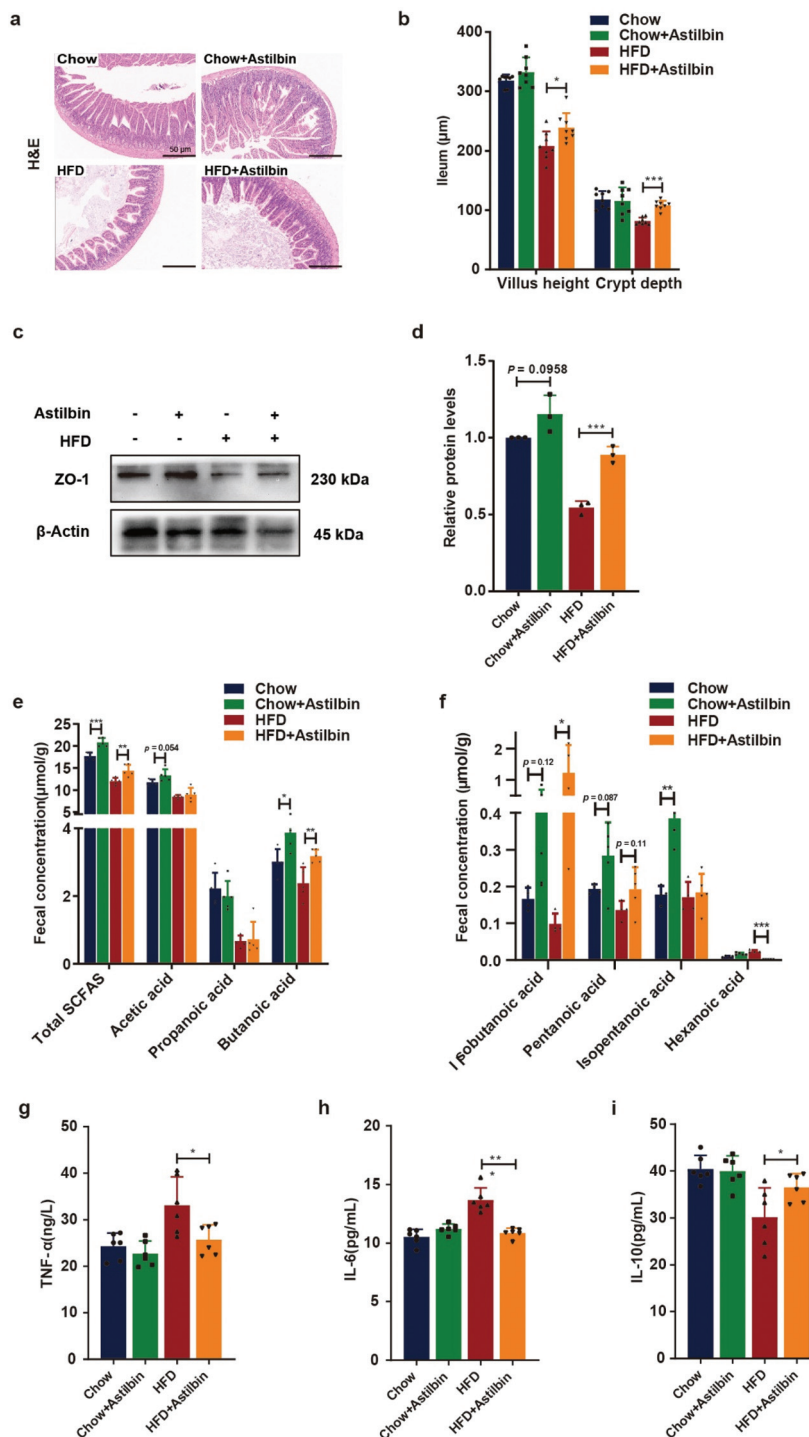


**Fig. 4** Effects of astilbin consumption on HFD-induced intestinal damage, SCFA disorders, and systemic inflammation. (a) H&E staining of the ileum in the four groups of mice. (b) Villus height and crypt depth (μm) of the ileum. (c) Western blot analysis of the effect of astilbin on ZO-1 expression in the ileum. (d) GAPDH levels detected in parallel served as controls. (e and f) Levels of SCFAs in the feces. Levels of (g) TNF- $\alpha$ , (h) IL-6, and (i) IL-10 in serum.

and HFD + Astilbin groups demonstrated an inconsistency of the metabolic profile. Further analysis using the orthogonal projections to latent structures discriminant analysis (OPLS-DA) model, which is a supervised analysis technique, was conducted

with satisfactory discriminating ability to screen for metabolic differentials in the liver samples ( $R^2 X = 0.349$ ,  $R^2 Y = 0.983$ ,  $Q^2 = 0.816$ ), as shown in Fig. 6b. Permutation tests with 200 iterations were performed to avoid overfitting (Fig. S4b†). A volcano

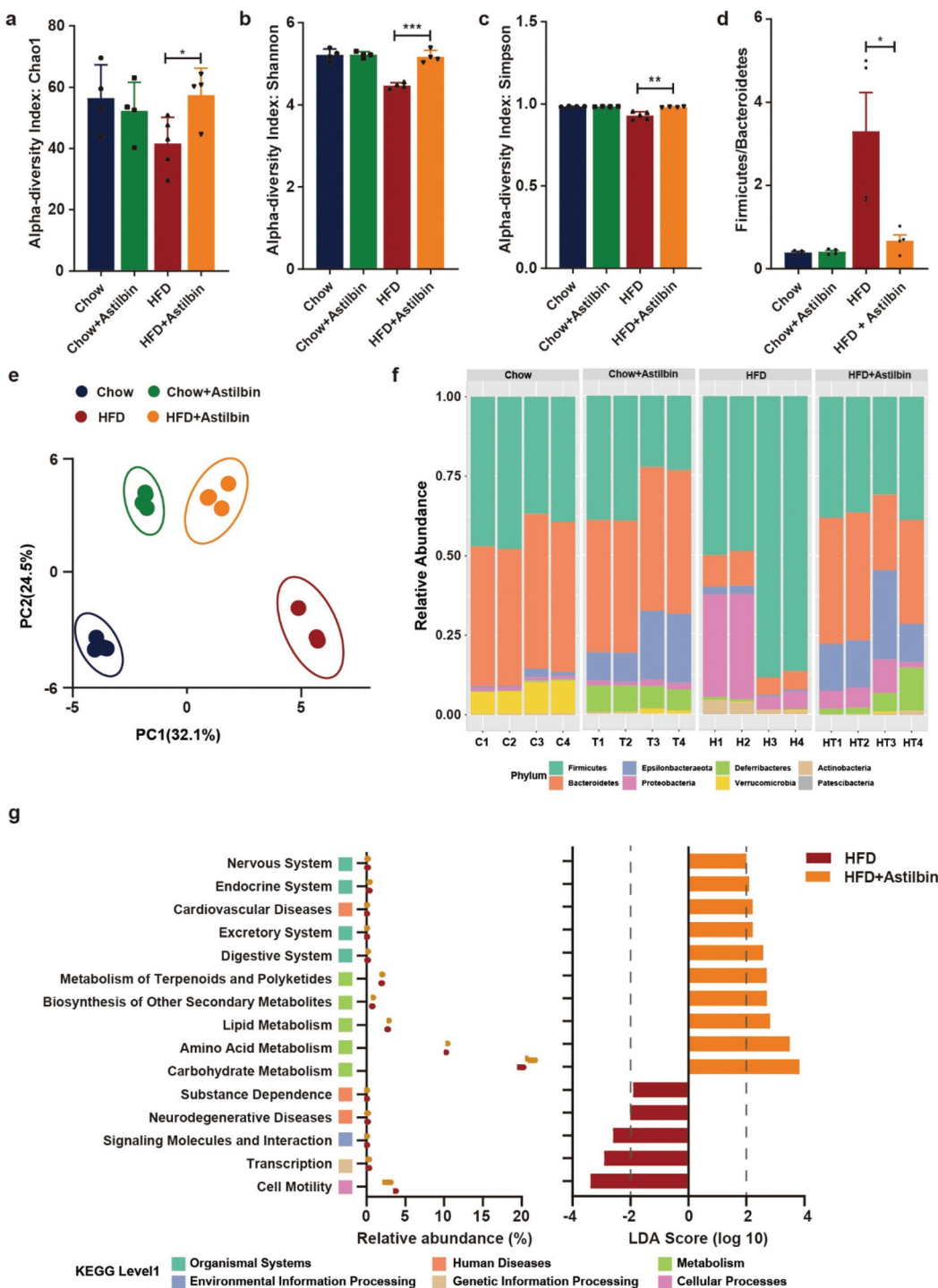


**Fig. 5** Astilbin altered the microbiota composition. (a–c) Fecal microbiota alpha-diversity. (d) Ratio of Firmicutes-to-Bacteroidetes. (e) Fecal microbiota beta diversity. (f) Bar graph of bacterial abundance at the phylum level. (g) LDA-based analysis of KEGG level 2 in the HFD + Astilbin group versus the HFD group significantly altered the pathway.

plot depicted significant metabolites with a  $P$  value  $<0.05$  and a fold-change value  $>1.5$  as the cutoff (Fig. 6c). As shown in Fig. S3c,† the levels of 27 metabolites were altered, of which the levels of 18 metabolites decreased and those of 9 metabolites increased, covering classes such as amino acids, carbohydrates,

and purines. The metabolites chosen for the heat map were evaluated according to: the fold change (FC)  $>1.5$ , VIP values  $>1$ , and a  $t$  test at the 95% level. Only the top 20 metabolites were selected for the Pearson hierarchical clustering. The results revealed significant differences in liver metabolites between the

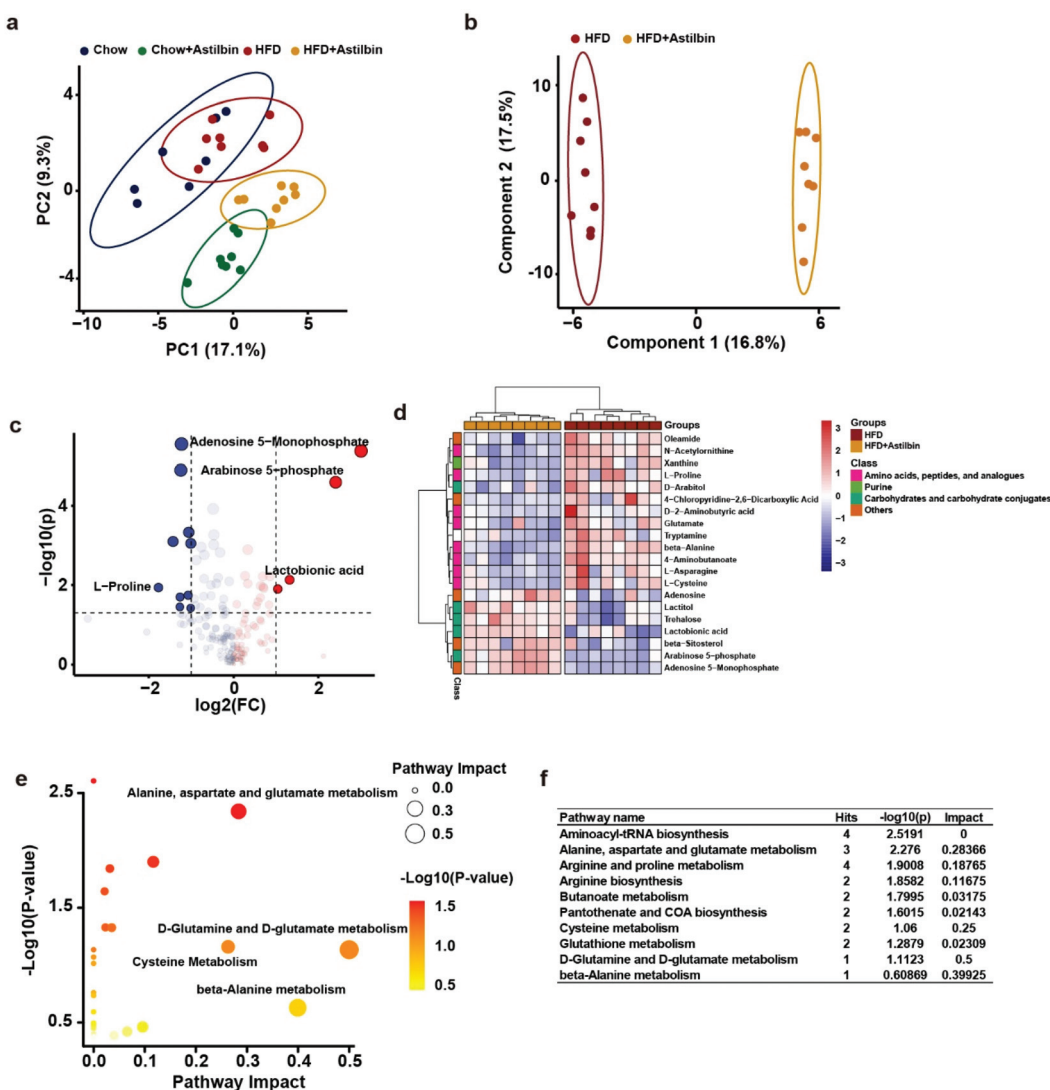


**Fig. 6** Effect of astilbin on liver metabolism in mice fed HFD. (a) PCA analysis of major sources of metabolite variability. (b) OPLS-DA analysis of metabolites between the HFD and HFD + Astilbin groups. (c) Volcano of metabolites. (d) Heat maps between the HFD and HFD + Astilbin groups, generated via the hierarchical Pearson clustering of metabolites, were selected based on a fold-change value  $>1.5$  and a t test at the 95% level. (e) Summary of the pathway enrichment analysis. (f) Metabolic pathway with significant trends.

two groups, which were consistent throughout with the outcomes of PCA and OPLS-DA (Fig. 6d).

Next, we used the MetaboAnalyst 5.0 online site to perform pathway enrichment for differential metabolites, which spanned amino acid metabolic pathways, energy metabolism pathways, lipid metabolism pathways, and purine metabolism pathways. Among all disturbed metabolic pathways, alanine, aspartate, and glutamate metabolism, D-glutamine and D-glutamate metabolism, and cysteine metabolism were most significantly altered (Fig. 6e and f).

### 3.7. Correlation of liver metabolites with particular bacterial OTUs

In order to investigate possible interaction pathways between intestinal microbiota and liver metabolism, we analyzed the

Pearson correlation coefficients between differential metabolites in the liver and differential OTUs at the genus level. As shown in Fig. 7, the levels of  $\beta$ -alanine and xanthine showed highly significant correlations ( $P < 0.01$ ) with 15 different OTUs at the genus level, more prominently positively correlated with *Coriobacteriaceae UCG-002*, *Ruminococcus torques* group, *Ruminococcaceae UCG-003* and *Ruminiclostridium 9* ( $P < 0.01$ ) and negatively correlated with *Alistipes* and *Muribaculum* ( $P < 0.01$ ). Meanwhile, levels of arabinose 5-phosphate and adenosine 5-monophosphate were found to show highly significant correlations ( $P < 0.05$ ) with 13 differential genus-level OTUs, with positive correlations ( $P < 0.01$ ) with *Alistipes* and *Muribaculum* and negative correlations with *Coriobacteriaceae UCG-002* and *Enterorhabdus* ( $P < 0.05$ ).

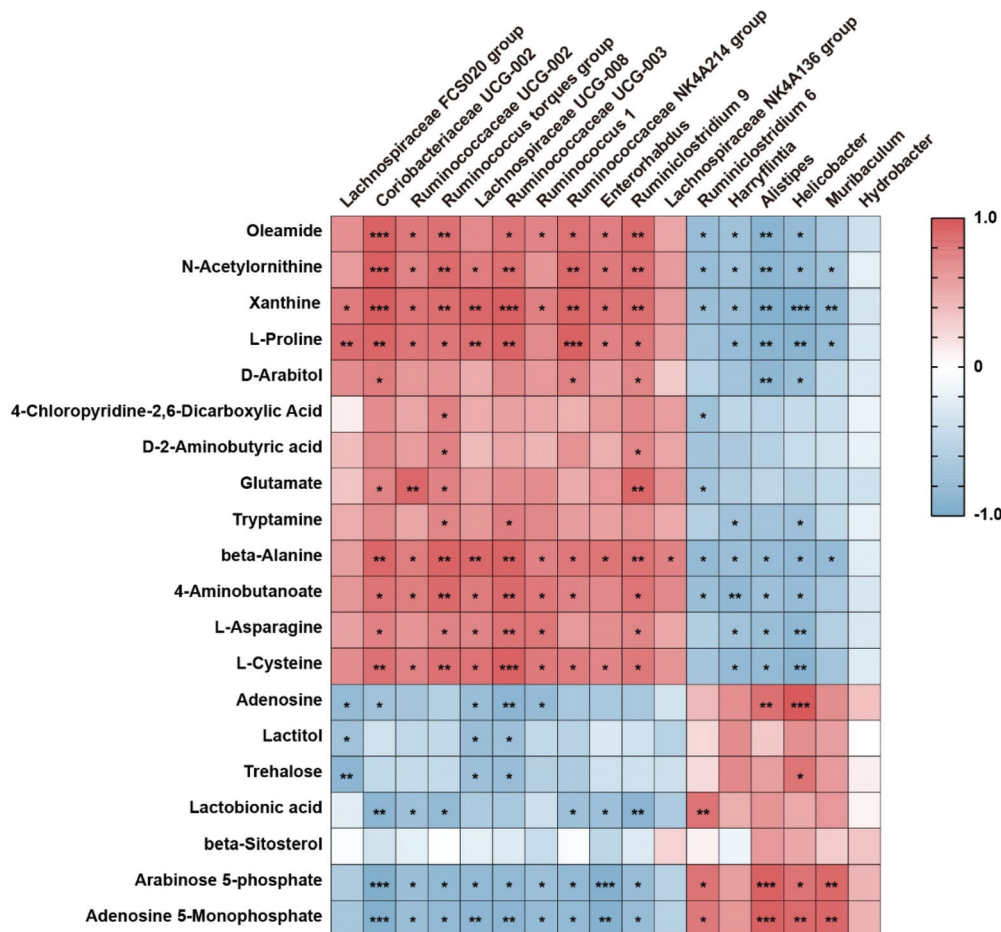


**Fig. 7** Heat map of the Pearson correlation between differential liver metabolites and differentiated bacterial OTUs at the genus level. Red represents a positive correlation and blue represents a negative correlation.

## 4. Discussion

Several studies showed that astilbin can reduce body weight and protect the liver in mice.<sup>14,15</sup> However, the impact of this flavonoid on the intestinal microbiota and the gut–liver axis was not investigated. In this study, we used astilbin extracted from *S. glabra* Roxb. to intervene in two dietary patterns of mice and studied the chronic physiological changes. The findings revealed that astilbin consumption significantly reduced the body weight of HFD mice, while body weight changes were insignificant after feeding a regular diet. Subsequently, the serum levels of TG in HFD mice also significantly reduced after the intake of astilbin. Several metabolic disorders (hyperglycemia, hypertriglyceridemia, and so on) associated with diabetes (and metabolic syndrome) are mechanistically linked to reduced blood levels of HDL cholesterol.<sup>25</sup> Interestingly, HDL levels significantly increased in both dietary mice after astilbin intervention, indicating the potential of astilbin to regulate lipid levels. In addition, the IPGTT results showed that astilbin was effective in improving glucose tolerance levels in HFD mice, which was consistent with previous reports in the literature.<sup>26</sup> Since the liver is the main organ of lipid metabolism,

we next examined lipid accumulation in the livers of mice. Oil Red staining and H&E staining showed that astilbin significantly reduced the number of hepatic lipid droplets and attenuated hepatic lipid accumulation in HFD mice. Meanwhile, the decrease in the AST and ALT levels, the marker enzymes of liver injury, also showed the outstanding ability of astilbin to protect the liver.

Astilbin selectively remodeled lipid classes in the livers of HFD mice, specifically glycerolipids and glycosphingolipids. Interesting changes in TAG lipids were observed in the HFD + Astilbin group compared with the HFD group. As the primary form of storage and transport of fatty acids in cells and plasma, triglycerides are stored in only limited quantities in the normal liver.<sup>27</sup> However, in the presence of overnutrition and obesity, liver fatty acid metabolism is altered, which usually leads to an excessive accumulation of triglycerides in liver cells, for which no effective therapy is available.<sup>27,28</sup> The accumulation of a large number of lipid droplets in liver cells is the main reason for liver steatosis; HFD causes the increase in the TAG level in the liver.<sup>29</sup> Notably, astilbin significantly reduced both liver and serum TAG levels in HFD mice, while no significant changes were observed in the mice fed a normal

diet. The analysis of fatty acyl chains showed that astilbin selectively and significantly reduced the levels of SFAs in the TAG species. Studies showed that SFA levels positively correlated with the development of inflammation;<sup>30</sup> the reduction in SFA levels in the HFD + Astilbin group also indicated the ability of astilbin to reduce liver inflammation.

Increased Firmicutes-to-Bacteroidetes ratio and the number of endotoxin-producing Proteobacteria characterize the intestinal microbiota of obese humans and HFD-fed mice,<sup>23,31</sup> suggesting that these major phyla may play an important role in obesity-associated inflammation. Astilbin consumption reduced the ratio of Firmicutes-to-Bacteroidetes and the number of Proteobacteria in HFD-fed mice to levels similar to those in chow-fed mice. Unexpectedly, astilbin increased the abundance and proportion of Epsilonbacteraeota in the microbiota of mice fed both diets. Although Epsilonbacteraeota increases the risk of peptic ulcer disease, it has been reported to provide some benefits, such as the reduced risk of obesity or childhood asthma.<sup>32,33</sup> *Alistipes* is associated with the production of acetate and propionate *in vivo* with potential anti-inflammatory effects. Epidemiological investigations have shown a significant reduction in the abundance of *Alistipes* with obesity and metabolic syndrome.<sup>34</sup> In addition, HFD has been shown to cause a decrease in the abundance of *Muribaculum* and an increase in the abundance of harmful bacteria such as *Lachnospiraceae FCS020* group, *Coriobacteriaceae UCG-002*, and *Lachnospiraceae UCG-008*.<sup>35,36</sup> Our results showed that astilbin supplementation increased the abundance of beneficial bacteria such as *Alistipes* and *Muribaculum* and decreased the abundance of harmful bacteria, suggesting that the effect of astilbin was, at least in part, to improve the microbial populations in HFD mice. Meanwhile, the results of pathway enrichment also showed an ameliorative effect of astilbin intake on carbohydrate metabolism, lipid metabolism, and digestive metabolism in HFD mice. These results suggested that astilbin as a prebiotic could be modulated in several ways to produce specific gut microbiota associated with reduced weight gain, inflammation, and increased lipid metabolism in obese patients.

The gut serves as the largest barrier between the host and its environment, protecting the host from a variety of ingested toxins and microorganisms.<sup>37</sup> The gut microbiota is closely related to the healthy function of the intestinal mucosal barrier, which is associated with metabolic health.<sup>38</sup> Increasing evidence suggests that HFD induces intestinal inflammation and enhances intestinal permeability by disrupting the intestinal microbial composition, leading to the disruption of the levels of internal environmental cytokines (*e.g.*, TNF- $\alpha$ , IL-6, and interferon-gamma).<sup>39</sup> After 9 weeks of astilbin consumption, we found that astilbin repaired the HFD damage to the intestinal mucosa and enhanced ZO-1 protein levels, thereby decreasing intestinal permeability to reduce pathogen-associated molecular patterns of escape into the bloodstream.<sup>38</sup> Moreover, astilbin consumption also increased the levels of SCFAs in the feces. SCFAs play a regulatory role in peripheral and central metabolism as key signaling molecules

produced by microbiota fermentation of nondigestible carbohydrates.<sup>40</sup> Among all SCFAs, butyrate, which has important intestinal and immunomodulatory functions, has gained attention.<sup>41</sup> Significantly lower fecal butyrate levels were observed in obese patients, patients with type 2 diabetes mellitus, and HFD mice, along with a lower abundance of butyrate-producing bacteria.<sup>42,43</sup> Butyrate has anti-inflammatory properties and affects adipogenesis, showing a positive effect on body weight and insulin sensitivity after consumption.<sup>22,44</sup> Astilbin consumption significantly increased the levels of total SCFAs in the feces of HFD mice. Further analysis revealed that butanoic acid and isobutanoic acid contributed the most to the increase, while the same changes were observed in the mice fed a regular diet. At the same time, we confirmed that the levels of pro-inflammatory factors IL-6 and TNF- $\alpha$  decreased and the levels of the anti-inflammatory factor IL-10 increased in serum. Together, these results confirmed that astilbin could effectively protect the intestinal barrier and reduce the systemic inflammatory response; these effects of astilbin appeared to form a virtuous circle that promoted the beneficial effects on the body.

Next, the bioinformatic methods were used to map the biochemistry of liver characteristics so as to identify the metabolic pathways affected by astilbin. We found that astilbin consumption effectively alleviated HFD-induced disorders of amino acid metabolism, energy metabolism, and lipid metabolism in the liver. A total of 27 altered metabolites in the liver tissue were identified in the HFD + Astilbin group compared with the HFD group, spanning metabolic pathways such as alanine, aspartate, and glutamate metabolism, D-glutamine and D-glutamate metabolism,  $\beta$ -alanine metabolism, and cysteine metabolism. Glutamate metabolism-related pathways were most significantly perturbed by astilbin intervention, with L-cysteine and glutamate significantly reduced after astilbin intake in HFD mice, which are precursors for glutathione synthesis.<sup>45</sup> However, glutathione content in the liver showed an increasing trend (FC = 1.35,  $P$  = 0.44), indicating that astilbin had a strong effect on glutathione synthesis. Adenosine 5-monophosphate (AMP) is a breakdown product of ATP, which is further converted into adenosine in the body.<sup>46</sup> A significant increase in the levels of both AMP and adenosine was found in the liver of mice in the HFD + Astilbin group, confirming that astilbin enhanced the hepatic ATP conversion pathway in HFD mice. Several studies have confirmed that the gut microbiota can influence energy metabolism,<sup>47</sup> and upon correlation analysis we found that AMP and adenosine were significantly positively correlated with the abundance of *Alistipes* ( $r$  > 0.85,  $P$  < 0.01) and negatively correlated with *Coriobacteriaceae UCG-002*, *Lachnospiraceae UCG-008* and *Ruminococcaceae UCG-003* ( $r$  > 0.7,  $P$  < 0.05), implying a link between these four bacteria and astilbin's role in improving hepatic ATP metabolism. It has been reported that intestinal microbiota is associated with purine metabolism and that a high-fat diet leads to impaired xanthine metabolism, resulting in a rise in xanthine in obese mice with associated microbiota disorders.<sup>48</sup> We found that astilbin significantly reduced

xanthine in the livers of HFD fed mice, and more interestingly, xanthine in the liver was significantly positively correlated with the abundance of *Coriobacteriaceae UCG-002*, *Ruminococcaceae UCG-003* and *Ruminococcaceae NK4A214* group ( $r > 0.9$ ,  $P < 0.001$ ) and negatively correlated with *Alistipes* and *Muribaculum* ( $r > 0.8$ ,  $P < 0.05$ ). This stimulates the idea that astilbin may exert its anti-obesity effect by regulating the core target microorganisms such as *Alistipes*, *Muribaculum* and *Ruminococcaceae NK4A214* group to influence liver metabolism.

## 5. Conclusion

Our results demonstrated that astilbin extracted from *S. glabra* Roxb. caused a significant improvement in lipid metabolism in HFD-fed mice. Using a combined lipidomic, gut microbiota, and metabolomic approach, we found that astilbin could be used as a prebiotic to reduce weight gain, chronic inflammation, and insulin resistance in obese individuals and modify intestinal microbiota disorders, hepatic ATP synthesis, lipid metabolism, and xanthine metabolism. In addition, astilbin-induced microbial alterations were associated with changes in liver metabolites, which provides new insights into the mechanisms underlying the reduction of obesity by astilbin. These results suggested that astilbin attenuates HFD-induced fat deposition and metabolic disorders by modulating the gut microbiota, ATP metabolism and xanthine metabolism, providing a basis for the development of astilbin as a functional food. Future research is needed to further unravel the potential mechanisms between metabolism and the gut microbial profile.

## Author contributions

Xiulan Sun: study concept and design and funding acquisition; Tingwei Wang: data analysis and writing the draft of the manuscript; Yongli Ye: writing – review and editing; Jian Ji: data visualization; Shuang Zhang: software and data curation; Xingxing Yang: software and validation; Jiayuan Xu: data curation; Jia-Sheng Wang: study design; Zhiyuan Chen: funding acquisition; Bangen Xia: resources; Hongfang Shen: investigation; Ruowei Xia: investigation; and Wenqin Shi: software.

## Conflicts of interest

The authors declare that they have no competing interests.

## Acknowledgements

This work has been supported by the National Natural Science Foundation of China (32125031), the Zhejiang Provincial Major Research Program of Traditional Chinese Medicine (2018ZY012), and the Postgraduate Research & Practice Innovation Program of Jiangsu Province (KYCX20\_1871).

## References

- 1 GBD 2017 Diet Collaborators, Health effects of dietary risks in 195 countries, 1990–2017: a systematic analysis for the Global Burden of Disease Study 2017, *Lancet*, 2019, **393**, 1958–1972.
- 2 A. Mishra, *et al.*, Fasting-mimicking diet prevents high-fat diet effect on cardiometabolic risk and lifespan, *Nat. Metab.*, 2021, **3**, 1342–1356.
- 3 N. Lv, *et al.*, Behavioral lifestyle interventions for moderate and severe obesity: A systematic review, *Prev. Med.*, 2017, **100**, 180–193.
- 4 P. Schrauwen and K. R. Westerterp, The role of high-fat diets and physical activity in the regulation of body weight, *Br. J. Nutr.*, 2000, **84**, 417–427.
- 5 G. Lee, *et al.*, Distinct signatures of gut microbiome and metabolites associated with significant fibrosis in non-obese NAFLD, *Nat. Commun.*, 2020, **11**, 4982.
- 6 W. Fan and R. M. Evans, Exercise Mimetics: Impact on Health and Performance, *Cell Metab.*, 2017, **25**, 242–247.
- 7 A. Astrup, The role of dietary fat in obesity, *Semin. Vasc. Med.*, 2005, **5**, 40–47.
- 8 C. W. Su, *et al.*, Helminth-Induced and Th2-Dependent Alterations of the Gut Microbiota Attenuate Obesity Caused by High-Fat Diet, *Cell. Mol. Gastroenterol. Hepatol.*, 2020, **10**, 763–778.
- 9 J. M. Natividad, *et al.*, Bilophila wadsworthia aggravates high fat diet induced metabolic dysfunctions in mice, *Nat. Commun.*, 2018, **9**, 2802.
- 10 W. Choi, *et al.*, Serotonin signals through a gut-liver axis to regulate hepatic steatosis, *Nat. Commun.*, 2018, **9**, 4824.
- 11 B. Wang, *et al.*, A High-Fat Diet Increases Gut Microbiota Biodiversity and Energy Expenditure Due to Nutrient Difference, *Nutrients*, 2020, **12**, 3197.
- 12 Y. Shi, *et al.*, Protective Effects of Smilax glabra Roxb, Against Lead-Induced Renal Oxidative Stress, Inflammation and Apoptosis in Weaning Rats and HEK-293 Cells, *Front. Pharmacol.*, 2020, **11**, 556248.
- 13 L. Dong, *et al.*, Astilbin from Smilax glabra Roxb, Attenuates Inflammatory Responses in Complete Freund's Adjuvant-Induced Arthritis Rats, *J. Evidence-Based Complementary Altern. Med.*, 2017, **2017**, 8246420.
- 14 A. Sharma, S. Gupta, S. Chauhan, A. Nair and P. Sharma, Astilbin: a promising unexplored compound with multidimensional medicinal and health benefits, *Pharmacol. Res.*, 2020, **158**, 104894.
- 15 L. Yang, Y. Zhu, S. Zhong and G. Zheng, Astilbin lowers the effective caffeine dose for decreasing lipid accumulation via activating AMPK in high-fat diet-induced obese mice, *J. Sci. Food Agric.*, 2021, **101**, 573–581.
- 16 C. Liu, *et al.*, Study on fecal fermentation characteristics of aloe polysaccharides in vitro and their predictive modeling, *Carbohydr. Polym.*, 2021, **256**, 117571.
- 17 Y. Wu, K. Chen, G. Xing, L. Li, B. Ma, Z. Hu, *et al.*, Phospholipid remodeling is critical for stem cell pluripo-

- tency by facilitating mesenchymal-to-epithelial transition, *Sci. Adv.*, 2019, **5**, eaax7525.
- 18 Q. Xuan, *et al.*, Development of a High Coverage Pseudotargeted Lipidomics Method Based on Ultra-High Performance Liquid Chromatography-Mass Spectrometry, *Anal. Chem.*, 2018, **90**, 7608–7616.
- 19 L. Xu, X. Xu, X. Wu, H. Kuang and C. Xu, Sex-Dependent Environmental Health Risk Analysis of Flupyradifurone, *Environ. Sci. Technol.*, 2022, **56**, 1841–1853.
- 20 T. Wang, *et al.*, Untargeted metabolomics analysis by gas chromatography/time-of-flight mass spectrometry of human serum from methamphetamine abusers, *Addict. Biol.*, 2021, **26**, e13062.
- 21 Z. Xu, *et al.*, Cold-induced lipid dynamics and transcriptional programs in white adipose tissue, *BMC Biol.*, 2019, **17**, 74.
- 22 E. E. Blaak, *et al.*, Short chain fatty acids in human gut and metabolic health, *Benefic. Microbes*, 2020, **11**, 411–455.
- 23 C. J. Chang, *et al.*, Ganoderma lucidum reduces obesity in mice by modulating the composition of the gut microbiota, *Nat. Commun.*, 2015, **6**, 7489.
- 24 P. Wang, *et al.*, Resveratrol reduces obesity in high-fat diet-fed mice via modulating the composition and metabolic function of the gut microbiota, *Free Radicals Biol. Med.*, 2020, **156**, 83–98.
- 25 P. Vollenweider, A. von Eckardstein and C. Widmann, HDLs, diabetes, and metabolic syndrome, *Handb. Exp. Pharmacol.*, 2015, **224**, 405–421.
- 26 G. S. Li, *et al.*, Effect of astilbin on experimental diabetic nephropathy in vivo and in vitro, *Planta Med.*, 2009, **75**, 1470–1475.
- 27 M. Alves-Bezerra and D. E. Cohen, Triglyceride Metabolism in the Liver, *Compr. Physiol.*, 2017, **8**, 1–8.
- 28 A. L. Birkenfeld and G. I. Shulman, Nonalcoholic fatty liver disease, hepatic insulin resistance, and type 2 diabetes, *Hepatology*, 2014, **59**, 713–723.
- 29 D. G. Mashek, Hepatic lipid droplets: A balancing act between energy storage and metabolic dysfunction in NAFLD, *Mol. Metab.*, 2021, **50**, 101115.
- 30 G. Ravaut, A. Légiot, K. F. Bergeron and C. Mounier, Monounsaturated Fatty Acids in Obesity-Related Inflammation, *Int. J. Mol. Sci.*, 2020, **22**, 330.
- 31 R. E. Ley, P. J. Turnbaugh, S. Klein and J. I. Gordon, Microbial ecology: human gut microbes associated with obesity, *Nature*, 2006, **444**, 1022–1023.
- 32 T. L. Cover and M. J. Blaser, Helicobacter pylori in health and disease, *Gastroenterology*, 2009, **136**, 1863–1873.
- 33 D. Y. Graham, Helicobacter pylori update: gastric cancer, reliable therapy, and possible benefits, *Gastroenterology*, 2015, **148**, 719–731.
- 34 B. J. Parker, P. A. Wearsch, A. Veloo and A. Rodriguez-Palacios, The Genus Alistipes: Gut Bacteria With Emerging Implications to Inflammation, Cancer, and Mental Health, *Front. Immunol.*, 2020, **11**, 906.
- 35 M. P. McNamara, *et al.*, Early-life effects of juvenile Western diet and exercise on adult gut microbiome composition in mice, *J. Exp. Biol.*, 2021, **224**, jeb239699.
- 36 J. Huang, *et al.*, In vitro fermentation of O-acetyl-arabinoolylan from bamboo shavings by human colonic microbiota, *Int. J. Biol. Macromol.*, 2019, **125**, 27–34.
- 37 M. W. Rohr, C. A. Narasimhulu, T. A. Rudeski-Rohr and S. Parthasarathy, Negative Effects of a High-Fat Diet on Intestinal Permeability: A Review, *Adv. Nutr.*, 2020, **11**, 77–91.
- 38 D. Zhou, *et al.*, Sodium butyrate attenuates high-fat diet-induced steatohepatitis in mice by improving gut microbiota and gastrointestinal barrier, *World J. Gastroenterol.*, 2017, **23**, 60–75.
- 39 A. P. Moreira, T. F. Texeira, A. B. Ferreira, M. C. Peluzio and R. C. Alfenas, Influence of a high-fat diet on gut microbiota, intestinal permeability and metabolic endotoxaemia, *Br. J. Nutr.*, 2012, **108**, 801–809.
- 40 D. J. Morrison and T. Preston, Formation of short chain fatty acids by the gut microbiota and their impact on human metabolism, *Gut Microbes*, 2016, **7**, 189–200.
- 41 C. Martin-Gallausiaux, L. Marinelli, H. M. Blottière, P. Larraufie and N. Lapaque, SCFA: mechanisms and functional importance in the gut, *Proc. Nutr. Soc.*, 2021, **80**, 37–49.
- 42 M. Elli, O. Colombo and A. Tagliabue, A common core microbiota between obese individuals and their lean relatives? Evaluation of the predisposition to obesity on the basis of the fecal microflora profile, *Med. Hypotheses*, 2010, **75**, 350–352.
- 43 J. Qin, *et al.*, A metagenome-wide association study of gut microbiota in type 2 diabetes, *Nature*, 2012, **490**, 55–60.
- 44 C. E. Pelgrim, *et al.*, Butyrate Reduces HFD-Induced Adipocyte Hypertrophy and Metabolic Risk Factors in Obese LDLr-/-Leiden Mice, *Nutrients*, 2017, **9**, 714.
- 45 J. Yin, *et al.*, L-Cysteine metabolism and its nutritional implications, *Mol. Nutr. Food Res.*, 2016, **60**, 134–146.
- 46 Y. Kondo, *et al.*, Adenosine 5'-Monophosphate Protects from Hypoxia by Lowering Mitochondrial Metabolism and Oxygen Demand, *Shock*, 2020, **54**, 237–244.
- 47 J. Nana, L. Xiaoxia, J. Mingliang, Y. Xingbin, H. Xin, L. Caiyan, *et al.*, Fubrick tea attenuates high-fat diet induced fat deposition and metabolic disorder by regulating gut microbiota and caffeine metabolism, *Food Funct.*, 2020, **11**, 6971–6986.
- 48 B. Wei, S. Wang, Y. Wang, S. Ke, W. Jin, J. Chen, *et al.*, Gut microbiota-mediated xanthine metabolism is associated with resistance to high-fat diet-induced obesity, *J. Nutr. Biochem.*, 2021, **88**, 108533.